Title

Differential gene expression profiling of functionally and developmentally distinct human prostate epithelial populations

Journal

The Prostate, 75(7)

ISSN

0270-4137

Authors

Liu, Haibo

Cadaneanu, Radu M

Lai, Kevin

et al.

Publication Date

2015-05-01

DOI

10.1002/pros.22959

Peer reviewed

The Prostate 75:764–776 (2015)

Differential Gene Expression Profiling of Functionally and Developmentally Distinct Human Prostate Epithelial Populations

Haibo Liu,[1,2] Radu M. Cadaneanu,[1,2] Kevin Lai,[1,2] Baohui Zhang,[1,2] Lihong Huo,[1,2] Dong Sun An,[2,3,4] Xinmin Li,[2,5] Michael S. Lewis,[6] and Isla P. Garraway[1,2,4,6]*

[1]*Department of Urology, David Geffen School of Medicine at UCLA, Los Angeles, California*
[2]*Jonsson Comprehensive Cancer Center, UCLA, Los Angeles, California*
[3]*UCLA School of Nursing, Los Angeles, California*
[4]*Broad Stem Cell Center, UCLA, Los Angeles, California*
[5]*Department of Pathology and Laboratory Medicine, David Geffen School of Medicine at UCLA, Los Angeles, California*
[6]*West Los Angeles VA Hospital, Greater Los Angeles Veterans Affairs Healthcare System, Los Angeles, California*

BACKGROUND. Human fetal prostate buds appear in the 10th gestational week as solid cords, which branch and form lumens in response to androgen [1]. Previous in vivo analysis of prostate epithelia isolated from benign prostatectomy specimens indicated that $Epcam^{+}CD44^{-}CD49f^{Hi}$ basal cells possess efficient tubule initiation capability relative to other subpopulations [2]. Stromal interactions and branching morphogenesis displayed by adult tubule-initiating cells (TIC) are reminiscent of fetal prostate development. In the current study, we evaluated in vivo tubule initiation by human fetal prostate cells and determined expression profiles of fetal and adult epithelial subpopulations in an effort to identify pathways used by TIC.

METHODS. Immunostaining and FACS analysis based on Epcam, CD44, and CD49f expression demonstrated the majority (99.9%) of fetal prostate epithelial cells (FC) were $Epcam^{+}CD44^{-}$ with variable levels of CD49f expression. Fetal populations isolated via cell sorting were implanted into immunocompromised mice. Total RNA isolation from $Epcam^{+}CD44^{-}CD49f^{Hi}$ FC, adult $Epcam^{+}CD44^{-}CD49f^{Hi}$ TIC, $Epcam^{+}CD44^{+}CD49f^{Hi}$ basal cells (BC), and $Epcam^{+}CD44^{-}CD49f^{Lo}$ luminal cells (LC) was performed, followed by microarray analysis of 19 samples using the Affymetrix Gene Chip Human U133 Plus 2.0 Array. Data was analyzed using Partek Genomics Suite Version 6.4. Genes selected showed >2-fold difference in expression and $P < 5.00E\text{-}2$. Results were validated with RT-PCR.

RESULTS. Grafts retrieved from $Epcam^{+}CD44^{-}$ fetal cell implants displayed tubule formation with differentiation into basal and luminal compartments, while only stromal

[This article was corrected on 19 March 2015 after original online publication. Table 1 had an incorrect gene list.]

Grant sponsor: National Institutes of Health awards; Grant numbers: CA-16042; AI-28697 U54 CA 143931; Grant sponsor: Department of Defense; Grant number: PC073073; Grant sponsor: Prostate Cancer Foundation Challenge and Young Investigator Awards; Grant sponsor: Jean Perkins Foundation; Grant sponsor: Margaret E. Early Medical Research Trust.

*Correspondence to: Isla P. Garraway, Department of Urology, David Geffen School of Medicine at University of California, Los Angeles, CA, USA. E-mail: igarraway@mednet.ucla.edu

Received 29 August 2014; Accepted 5 December 2014
DOI 10.1002/pros.22959
Published online 7 February 2015 in Wiley Online Library (wileyonlinelibrary.com).

outgrowths were recovered from Epcam- fetal cell implants. Hierarchical clustering revealed four distinct groups determined by antigenic profile (TIC, BC, LC) and developmental stage (FC). TIC and BC displayed basal gene expression profiles, while LC expressed secretory genes. FC had a unique profile with the most similarities to adult TIC. Functional, network, and canonical pathway identification using Ingenuity Pathway Analysis Version 7.6 compiled genes with the highest differential expression (TIC relative to BC or LC). Many of these genes were found to be significantly associated with prostate tumorigenesis.

CONCLUSIONS. Our results demonstrate clustering gene expression profiles of FC and adult TIC. Pathways associated with TIC are known to be deregulated in cancer, suggesting a cell-of-origin role for TIC versus re-emergence of pathways common to these cells in tumorigenesis. *Prostate 75:764–776, 2015.*

KEY WORDS: **human prostate epithelial microarray; fetal prostate; prostate stem cell; basal cell; prostate tissue regeneration; prostate tubule initiation**

INTRODUCTION

Prostate organogenesis coincides with fetal testes secretion of testosterone, its conversion to dihydrotestosterone (DHT) and binding of the androgen receptor (AR) to cells within the urogenital sinus mesenchyme (UGSM) [1]. These stromal events initiate epithelial outgrowth in the form of solid prostatic buds, which eventually elongate, canalize, and differentiate into branching ductal/acinar structures composed of basal and luminal (secretory) epithelial compartments [2,3]. Fetal prostate development is relatively static until approximately 24 weeks gestation, when a rapid increase in T is paralleled by exponential prostatic growth that persists into the postnatal period. At mid-gestation, when androgen levels are relatively low (14–20 weeks), prostatic buds arise from the wall of the UGS and are composed of epithelia possessing an expression profile that resembles adult basal cells (androgen receptor (AR)-negative, P63-positive, cytokeratin (CK) 5-positive) [4]. Human prostate tissue regeneration studies have demonstrated that adult basal cells are capable of surviving in castrate environments and include a subset of cells that are capable of inducing tubule-initiation, branching morphogenesis, and formation of ducts/acini containing differentiated basal and luminal compartments [4–9]. Characterization of epithelial cells isolated from fetal prostate tissue may allow further insight into adult prostate cellular hierarchy, as well as illuminate shared mechanisms used in fetal prostate development and adult prostate glandular maintenance that could be co-opted in tumorigenesis.

In several tissues (e.g., breast, lung, prostate), the cells of origin where tumor initiation occurs display stem/progenitor properties, including self-renewal, proliferation, differentiation, and the ability to interact with the stroma to create a vascularized niche in vivo [10–13]. In models of human prostate tumorigenesis, basal cells display these features and also appear to be cells of origin of prostate cancer, since introduction of genetic alterations (AKT, ERG, and AR overexpression) followed by tissue recombination yields foci of adenocarcinoma within the recombinant grafts [11]. Although murine studies suggest that luminal cells have tumor-initiating potential, such observations have yet to be demonstrated with primary human cells that display a luminal profile [11,14].

Our previous studies indicate that the $Epcam^{+}CD44^{-}CD49f^{Hi}$ basal subpopulation displays superior tubule initiation capability in vivo, relative toother prostate epithelial subpopulations [15]. Compared to terminally differentiated $Epcam^{+}CD44^{-}CD49f^{Lo}$ luminal cells (LC) that express mature prostatic markers including androgen receptor (AR) and prostate specific antigen (PSA), $Epcam^{+}CD44^{-}CD49f^{Hi}$ TIC express basal markers (i.e., P63, CK5) and possess self-renewal and differentiation capabilities [5,15]. Determination of surface marker and gene expression profiles of prostate epithelial populations that have distinctive functional capabilities may help to uncover mechanisms involved in ductal/acini development, maintenance, and expansion.

In our study, the antigenic profile of fetal prostate buds was analyzed via immunohistochemistry (IHC) and fluorescent-activated cell sorting (FACS) and compared with benign adult prostate tissues. Fractionation of dissociated fetal prostate specimens based on Epcam/CD44 expression allowed quantitation and functional evaluation of specific prostate cell populations. In an effort to identify genes and molecular pathways associated with fetal and adult epithelial subpopulations isolated based upon basal/luminal compartment, developmental stage, and/or functional capabilities,

the Affymetrix Gene Chip Human U133 Plus 2.0 Array was utilized to conductgenome-wide expression profiling and comparative analysis. Data analysis was designed to gain further understanding of the pathways that may support tubule initiation, branching morphogenesis, cell survival, and angiogenesis processes, which are likely to be intimately related to tumorigenesis.

MATERIALS and METHODS

Human Subjects and Tissue Samples

Human prostate tissue was obtained following a research protocol that was approved by the Office for the Protection of Research Subjects at UCLA and the Greater Los Angeles VA Medical Center. Informed consent was obtained on all participants if identifying information was included. Many cases are procured without identifying information in an anonymous fashion at UCLA, therefore, an approved Institutional Review Board protocol with written consent was not required by the Office for the Protection of Research Subjects. Fetal prostate samples (approximately 14–18 weeks gestation) were obtained in accordance with federal and state guidelines, and prostate tissue was used for frozen/paraffin blocks or dissociated in order to obtain single cell suspensions as previously described [15]. A total of 9 adult and 30 fetal samples were used in this analysis. Adult prostate tissues procured from surgical specimens were divided and adjacent tissue sections were snap frozen in liquid-nitrogen and/or formalin-fixed and paraffin-embedded for histological analysis. A genitourinary pathologist designated benign regions, and fresh tissue specimens were matched with adjacent frozen section slides to enable macrodissection and isolation of benign tissues. Mechanical and enzymatic digestion was performed to generate organoids that were sequentially filtered through 100- and 40-μm cell strainers as previously described [5]. Repeated passage through a 23-gauge needle enabled single cell suspensions to be generated. Cells were counted and resuspended in RPMI supplemented with 10% FBS, followed by immediate cell sorting. Fresh hFPS cells were cultured in RPMI supplemented with 10% FBS and R1881 (Sigma) and passaged three times prior to use in tissue regeneration assays.

Immunohistochemistry

Formalin-fixed and paraffin-embedded tissue blocks were cut into four-micron thick sections. Deparaffinization with xylene and rehydration via a descending series of ethanol washes was performed, followed by antigen retrieval and standard immunoperoxidase procedures using primary antibodies as previously described [5]. Antibodies used for IHC included CK5 (Convance), CK8 (Zymed), CK19 (eBioscience), P63 (Santa Cruz), CD44 (eBioscience), AR (Santa Cruz), and PSA (Dako).

Fluorescence-Activated Cell Sorting (FACS)

Single cells were suspended in PBS, 2 mM EDTA, 0.5% BSA and stained with antibody for 15 min at 4°C. Fluorescence-activated cell sorting and analysis were performed on a BD Special Order FACS Aria II system and Diva v6.1.1 (BD Biosciences). Live single cells were gated based on scatter properties and analyzed for their surface marker expression as previously described [15]. Antibodies used for FACS include Epcam-PE (Miltenyi Biotech), CD44-FITC (ebioscience), and CD49f-APC (BioLegend).

Prostate Tissue Regeneration in Immunocompromised Mice

In vivo tissue regeneration experiments were performed in male SCID-NOD^{IL2grNULL} mice in accordance with protocol number 2007–189-13, approved by the Animal Research Committee within the Office for the Protection of Research Subjects at UCLA. Mice (6–8 weeks old) were subjected to subcutaneous injections of fractionated fetal prostate cells. Fetal cells were pooled from dissociated fetal tissues. Epcam^{+}CD44^{-} fractions were collected (3×10^3 to 5×10^3 cells) or Epcam^{-}CD44^{-} fractions (5×10^3 to 1×10^4 cells). Cell fractions were combined with 2× hFPS. The epithelial and stromal cells were suspended in Matrigel® and subcutaneously implanted as previously described [5]. A total of eight recombinants in Matrigel were implanted in to immunocompromised mice, four implants per cell fraction. Time-release testosterone pellets (Innovative Research of America) were simultaneously implanted. Grafts were retrieved after 16 weeks, and paraffin-embedded sections were generated for immunohistochemical analysis. Grafts were retrieved at a frequency of 75% (total of 6 grafts retrieved for analysis).

RNA Isolation and Microarray Hybridization

RNA was extracted using Qiagen RNAeasy® Micro Kit, following the manufacturer's instructions. After RNA extraction, all quantitation and microarray experiments were performed at the UCLA Department of Pathology Clinical Microarray Core Laboratory. RNA integrity was analyzed using an Agilent 2100 Bioanalyzer (Agilent Technologies, Palo Alto,

CA). RNA purity and concentration was determined using a Nanodrop 8000 (Nanodrop Products, Wilmington, DE). Microarray targets were generated using FL-Ovation cDNA Biotin Module V2 (NuGen Technologies, San Carlos, CA) and then hybridized to the Affymetrix Gene Chip U133Plus 2.0 Array (Affymetrix, Santa Clara, CA), all according to the manufacturer's instructions. The arrays were washed and stained with streptavidin phycoerythrin in Affymetrix GeneChip protocol, and then scanned using an Affymetrix GeneChip Scanner 3000.

Microarray Data Analysis

AGCC software (Affymetrix) was utilized for acquisition of array images and initial quantification. For subsequent data analyses (cluster and principle component analyses), the Partek Genomics Suite Version 6.4 (Partek, St. Louis, MO) was employed and conducted using Partek default settings. Differentially expressed genes were selected at $\geq$2-fold difference (comparing various prostate subpopulations) and $P < 5.00\text{E-}2$. Biofunctional analysis was performed using Ingenuity Pathways Analysis software Version 7.6 (Ingenuity Systems, Redwood City, CA) as previously described [16,17].

RT-PCR Analysis

For quantitative Real-time PCR, RNA was generated using Qiagen RNAeasy Micro Kit, following the manufacturer's instructions. The concentration and purity of total RNA was assessed via UV spectrophotometer (260 and 280 nm). Total RNA (up to 5 μg) was used to generate cDNA via SuperScript III First-Strand Synthesis Kit (Invitrogen). For quantitative Real-time PCR, SYBR®-Green Supermix (Bio-Rad Laboratories) was utilized with a Bio-Rad CFX Multicolor Real-time PCR detection system. PCR primer pairs for PSA, AR and p63 were purchased from SABiosciences Corporation. The PCR reaction conditions were performed as previously described [15].

RESULTS

Evaluation of Basal and Luminal Marker Expression in Fetal and Adult Prostate Tissue

In order to evaluate the expression profile of prostate buds and developing ducts/acini that are present during the mid-gestational, low androgen phase of fetal development, immunohistochemical (IHC) staining was performed on formalin-fixed, paraffin-embedded tissue sections derived from autoptic fetal prostate (14–18 week gestation). Benign adult prostate tissue, procured from prostatectomy specimens, was stained for comparative analysis. The general epithelial marker, Epcam, was detected in both fetal and adult prostate epithelia (Fig. 1A). Epcam staining appeared stronger in adult tissues (3+) than fetal tissues (1+). Consistent with previous studies, adult prostate acini demonstrated a well-demarcated basal compartment, designated by strong (3+) CK5, P63, and CD44 co-expression (Fig. 1B). Basal markers CK5 and P63 demonstrated abundant (3+ staining) throughout fetal prostate acini. In contrast, luminal markers CK8 and AR staining ranged from low (+/−) to undetectable (−) in fetal epithelia (Fig. 1D). However, fetal stromal cells surrounding the epithelial buds displayed strong (3+) AR expression relative to adult stroma, which displayed low AR (+/−) staining (Fig. 1D).

Previous studies of prostate epithelial compartments have indicated that there may be intermediate cells that may express specific cytokeratins, including CK19 [18]. Intermediate cells may represent transit amplifying progenitor cells that eventually mature into secretory (luminal) cells [19]. We evaluated the expression of CK19 and found 3+ staining predominantly within basal cells in adult prostate tissue specimens (Fig. 1C). Fetal prostate epithelial demonstrated pan-epithelial staining of CK19(3+).

In contrast to adult prostate tubules which exhibit discreet basal ($CK5^+P63^+CD44^+CK8^-AR^-$) and luminal ($CK5^-P63^-CD44^-CK8^+AR^+$) compartments, developing acinar structures in the fetal prostate displayed a predominantly basal profile, with the exception of CD44 expression, which appeared low to undetectable (+/−) in the majority of fetal epithelial cells relative to adult basal cells (Fig. 1B). Interestingly, this fetal epithelial IHC profile ($Epcam^+CK5^+P63^+CD44^-CK8^-AR^-$) matches that of a small subset of adult basal TIC [4,5,15].

Cell Sorting of Epithelial and Stroma Populations Isolated From Fetal Prostate Tissue

We have previously performed functional analysis of fractionated adult prostate epithelial cells using the combination of Epcam, CD44, and CD49f antibodies for cell sorting of dissociated benign tissue [15]. The $Epcam^+CD44^-CD49f^{Hi}$ (TIC) fraction has consistently demonstrated superior tubule-initiating activity compared to other cell fractions when these cells are recombined with stroma and implanted subcutaneously into immunocompromised mice [15]. In order to determine the antigenic profile of cell populations, FACS analysis of dissociated fetal prostate tissue specimens was performed. Distinct fetal prostate cell populations were isolated via cell sorting to assess

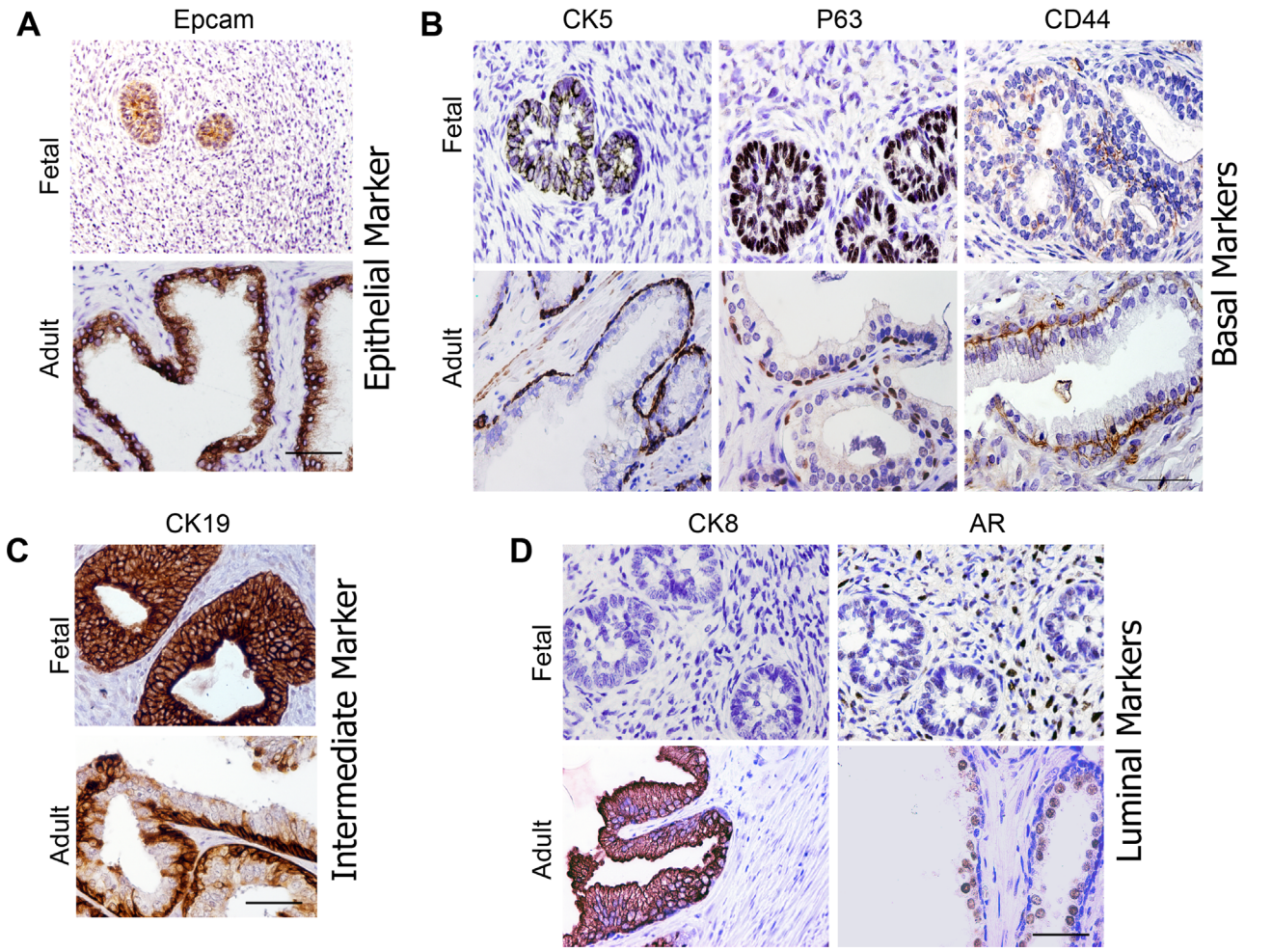

Fig. 1. Fetal prostate tissue is enriched with epithelial cells that display a marker profile similar to putative adult TIC. Immunohistochemical analysis of (**A**) epithelial cell marker, Epcam, (**B**) basal markers CK5, P63, and CD44, (**C**) intermediate marker, CK19, and (**D**) luminal markers CK8 and AR in human fetal prostate and benign adult prostate tissue specimens (40× magnification).

tubule-initiation capability, in vivo, and determine gene expression profiles via microarray analysis, (Fig. 2A). As suggested via IHC of fetal prostate tissue (Fig. 1A), Epcam is detected on the surface of fetal epithelial cells via FACS (Fig. 2B). However, the majority of fetal cells isolated from dissociated prostate tissue appeared to be $Epcam^{-}$ and likely represent stroma and blood cells (Fig. 2B) [15]. The FACS profile of dissociated fetal prostate tissue differs from the previously described profile of benign adult prostate, which includes abundant $Epcam^{+}CD44^{-}$ and $Epcam^{+}CD44^{+}$ populations [15]. The vast majority of fetal prostate epithelial cells appear to be $Epcam^{+}CD44^{-}$ (Fig. 2B). In fact, less than 0.1% of fetal prostate cells are $Epcam^{+}CD44^{+}$. This result is consistent with the IHC staining using CD44 antibodies (Fig. 1A). When $Epcam^{+}CD44^{-}$ fetal prostate cells are analyzed for CD49f expression, a spectrum of bright to dim cells are observed (Fig. 2B). Bright co-expression of CD49f enabled identification of an $Epcam^{+}CD44^{-}CD49f^{Hi}$ population [15], which is the antigenic profile of the adult TIC population.

$Epcam^{+}CD44^{-}$ and $Epcam^{-}CD44^{-}$ populations were collected from pooled dissociated fetal prostate tissue samples for comparative functional analysis in prostate tubule regeneration assays (Fig. 2C). Three dissociated fetal prostate samples were pooled prior to cell sorting in order to collect fractions for in vivo implantation. Fetal cell fractions were combined with cultured hFPS and implanted subcutaneously into NOD-SCID mice supplemented with testosterone, as previously described for adult prostate cell isolates [15]. Grafts were retrieved after approximately 16 weeks in vivo, followed by paraffin-embedding

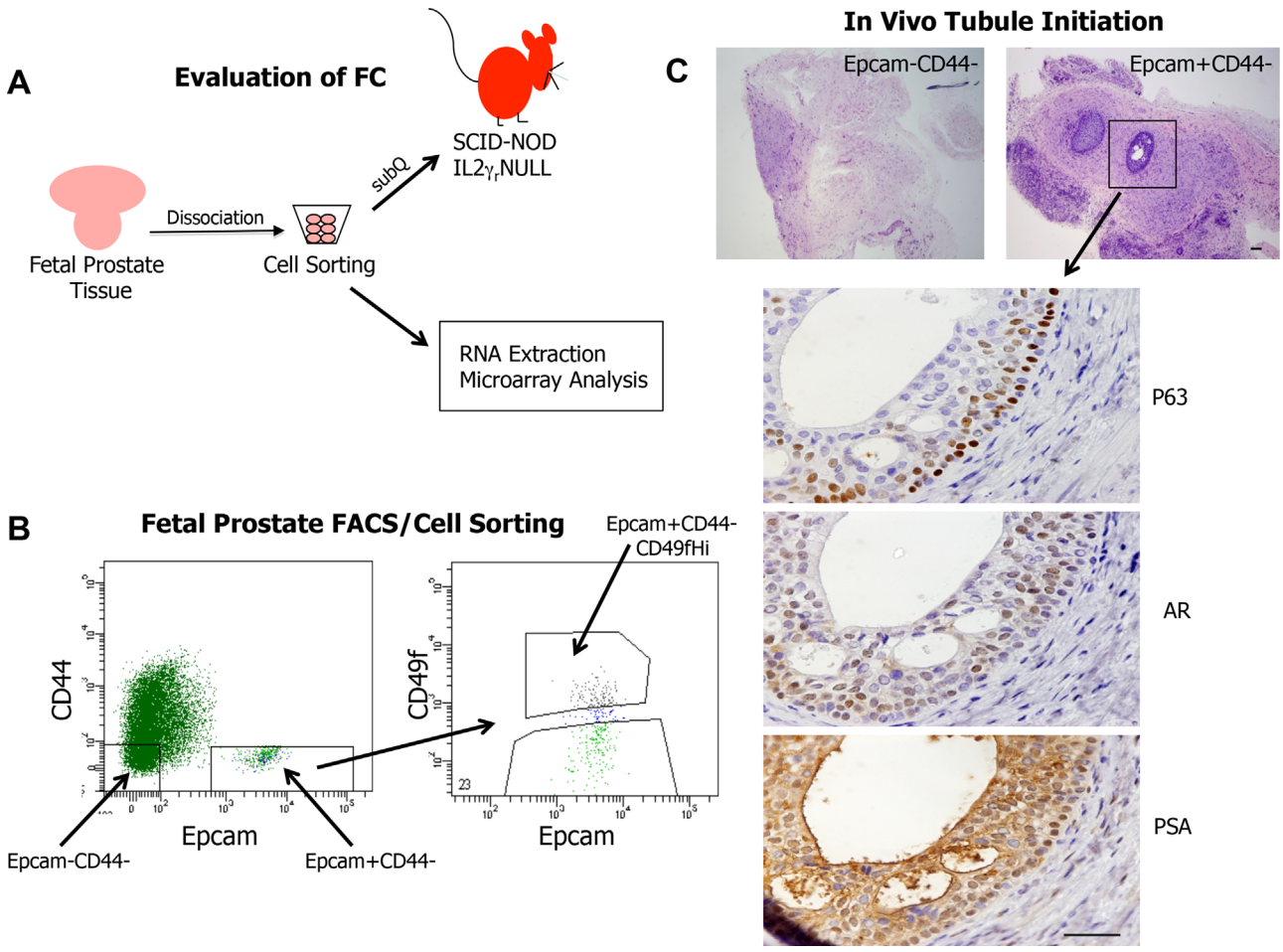

Fig. 2. Isolation and sorting of human fetal prostate cells for in vivo analysis and gene expression profiling. **A**: Schematic diagram demonstrating the approach for isolating prostate cells from fetal tissues for cell sorting and in vivo/in vitro analysis. **B**: FACS analysis of cells expressing Epcam, CD44, and CD49f collected from pooled dissociated human fetal prostate tissues. Total prostate cells were stained with Epcam-PE, CD44-FITC, and CD49f-APC conjugated antibodies prior to FACS analysis. $Epcam^{+}CD44^{+}$ cells are gated in order to evaluate CD49f expression within this population. C. H&E stained sections of paraffin-embedded 12-week grafts harvested from $SCID\text{-}NOD^{IL2\gamma rNULL}$ mice. $Epcam^{-}CD44^{-}$ (n = 4) or $Epcam^{+}CD44^{-}$ (n = 4) cell fractions were combined with hFPS and Matrigel® were implanted subcutaneously into male $SCID\text{-}NOD^{IL2\gamma rNULL}$ mice. Testosterone was supplemented via pellets inserted subcutaneously. Grafts induced by $Epcam^{+}CD44^{-}$ (FC) fraction demonstrate a basal layer adjacent to the surrounding stroma containing $P63^{+}AR^{-}$ PSA^{-} cells and secretory cells surrounding the lumen with a $P63^{-}AR^{+}PSA^{+}$ profile. Representative sections from tissue recombinants using fractionated fetal prostate cells are shown at 4× (H&E) and 40× (IHC) magnification.

and IHC analysis of tissue sections (Fig. 2C). $Epcam^{-}CD44^{-}$ fractions yielded grafts with stromal outgrowth, but no tubules were observed in 100% of grafts retrieved (Fig. 2C). On the other hand, one out of the four grafts retrieved from $Epcam^{+}CD44^{-}$ fractions displayed clear epithelial cords and acini surrounded by stroma (Fig. 2C). These structures appeared to differentiated, and included a $P63^{+}$ basal-like layer with predominant $AR^{+}PSA^{+}$ secretory cells surrounding the lumen (Fig. 2C). The multilayer appearance of the acini, however, suggests that differentiation was incomplete or did not accurately recapitulate normal adult bilayered ducts.

Hierarchical Clustering and Principal Component Analysis Demonstrate Distinctive Molecular Phenotypes Among Prostate Epithelial Subpopulations

In order to determine gene expression profiles of epithelial cell populations isolated based on Epcam/CD44/CD49f antigenic expression, total RNA was isolated from fractionated fetal or adult prostate cells for microarray analysis. The Affymetrix Gene Chip Human U133 Plus 2.0 array was used, which includes more than 54,000 probe sets that can analyze the relative expression of more the 47,000 transcripts with extensive

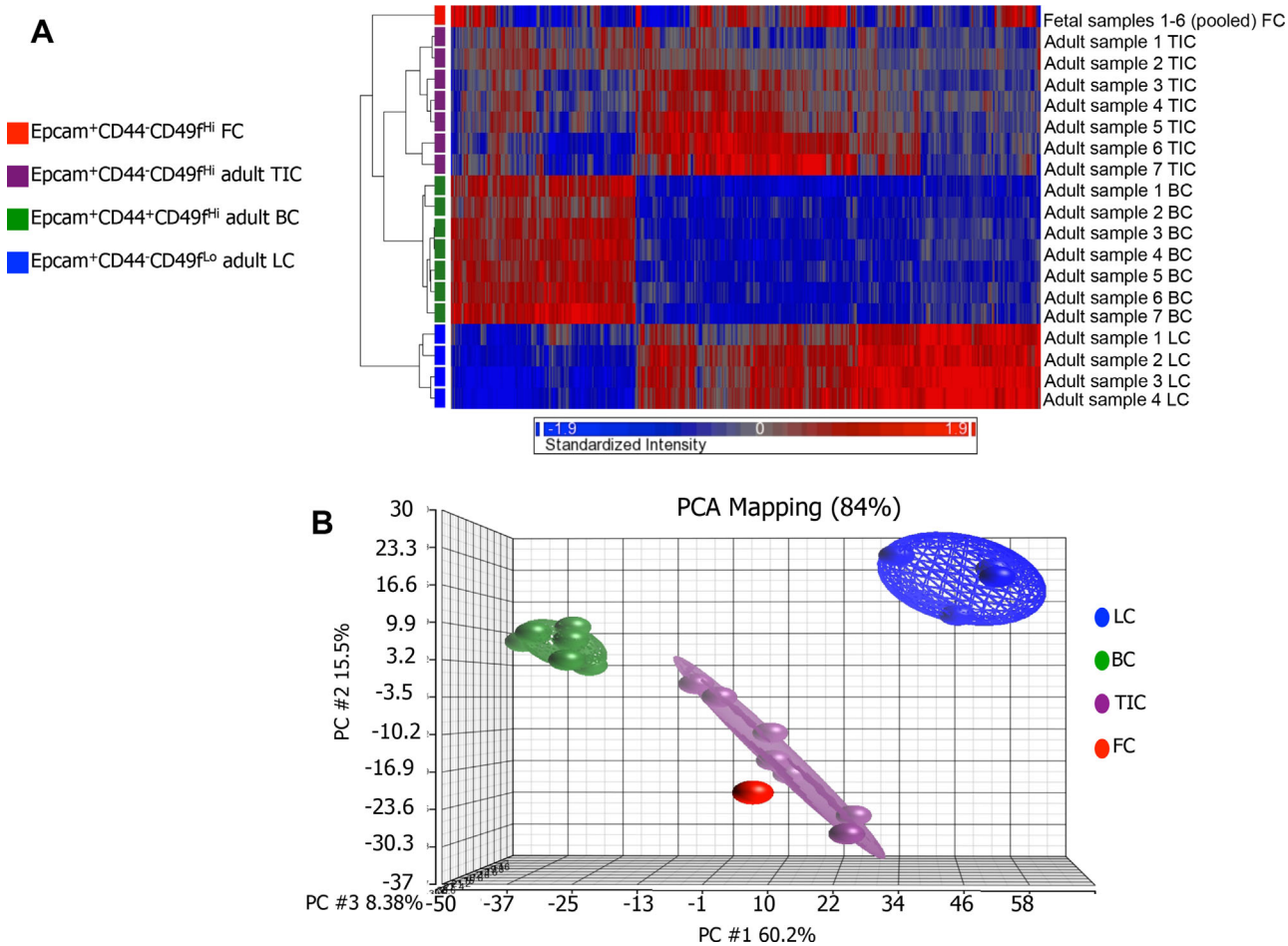

Fig. 3. Microarray analysis of functionally and developmentally distinct human prostate epithelial cell fractions. **A**. Hierarchical clustering of primary prostate cell fractions sorted from fetal or adult tissues. With the exception of the first row, which contains six pooled fetal samples (Fetal samples 1–6 (pooled) FC), each row represents an individual adult cell fraction and each column represents a single gene. On the hierarchical tree on the left side of the diagram, color coded boxes designate each cell population: the red box indicates the pooled FC (Epcam^{+}CD44^{-}CD49f^{Hi}), the purple boxes indicate TIC (Epcam^{+}CD44^{-}CD49f^{Hi}), green boxes indicate BC (Epcam^{+}CD44^{+}CD49f^{Hi}), and blue boxes indicate LC (Epcam^{+}CD44^{-}CD49f^{Lo}). Relative gene expressions are represented with red (higher-level expression), blue (lower level expression), and grey (no change). **B**. Principal component analysis of fetal and adult prostate cell fractions. Analysis of 19 samples resulted in four relatively distinct groups correlating with antigenic profiles of each cell fraction from adult and fetal tissues.

expression analysis of the entire genome. Fetal RNA from sorted cells (6 pooled fetal samples) was compared with RNA from individually sorted adult prostate cell fractions isolated from 12 patients (unpooled). In some cases, the RNA quantity and quality from certain adult fractions were not sufficient to proceed with Affymetrix array analysis, so these samples were not included. All together, 21 adult samples were analyzed, as well as Epcam^{+}CD44^{-}CD49f^{Hi} cell fractions from six fetal samples that were pooled together order to obtain sufficient RNA for gene expression analysis. Upon review, three of the adult samples appeared to be significant outliers and were removed from further analysis, leaving 19 remaining samples for comparison, including the pooled FC (Epcam^{+}CD44^{-}CD49f^{Hi}) sample, seven TIC (Epcam^{+}CD44^{-}CD49f^{Hi}), seven BC (Epcam^{+}CD44^{+}CD49f^{Hi}), and four LC (Epcam^{+}CD44^{-}CD49f^{Lo}).

A hierarchical clustering map was generated using these probes/genes of interest (Fig. 3A). Differentially expressed genes were defined by a *P*-value of <5.00E-2 and twofold or greater difference in relative expression between groups TIC versus LC and BC. This approach resulted in the segregation of 852 candidate probe sets developed on the basis of the statistical significance ($P < 5.00\text{E-}2$) of the difference in their expression of the study group (TIC versus LC + BC) and an at least two fold change in gene

TABLE I. SC Versus PC + LC

Probeset ID	Gene symbol	Gene name	Fold difference	*P*-value
Upregulated				
1552487_a_at	BNC1	basonuclin 1	6.99301	7.36E-08
229160_at	MUM1L1	melanoma associated antigen (mutated) 1-like 1	6.51144	0.000554755
228293_at	DEPDC7	DEP domain containing 7	6.44196	4.59E-07
201141_at	GPNMB	glycoprotein (transmembrane) nmb	5.83103	1.80E-06
230127_at	–	–	5.6681	2.21E-08
229290_at	DAPL1	death associated protein-like 1	5.51367	2.27E-05
204580_at	MMP12	matrix metallopeptidase 12 (macrophage elastase)	5.28229	4.12E-06
205828_at	MMP3	matrixmetallopeptidase 3 (stromelysin 1, progelatinase)	5.09891	7.07E-05
204135_at	FILIP1L	filamin A interacting protein 1-like	4.89582	1.36E-05
1554966_a_at	FILIP1L	filamin A interacting protein 1-like	4.81849	1.34E-05
241382_at	PCP4L1	Purkinje cell protein 4 like 1	4.79516	4.75E-06
220431_at	TMPRSS11E	transmembrane protease, serine 11E	4.59135	2.10E-05
240353_s_at	C12orf54	chromosome 12 open reading frame 54	4.54448	1.86E-07
1556793_a_at	FAM83C	family with sequence similarity 83, member C	4.41239	3.58E-06
209596_at	MXRA5	matrix-remodelling associated 5	4.40538	9.87E-09
226755_at	LOC642587	NPC-A-5	4.30913	8.65E-07
206030_at	ASPA	aspartoacylase	4.16302	4.10E-08
236220_at	–	–	4.15706	1.45E-05
233537_at	KRTAP3-1	keratin associated protein 3-1	4.12838	2.61E-06
210809_s_at	POSTN	periostin, osteoblast specific factor	4.00728	1.80E-05
238956_at	LOC100506781	hypothetical LOC100506781	3.98049	0.000165459
240354_at	C12orf54	chromosome 12 open reading frame 54	3.93021	8.45E-06
212977_at	CXCR7	chemokine (C-X-C motif) receptor 7	3.9302	0.000267768
222484_s_at	CXCL14	chemokine (C-X-C motif) ligand 14	3.9208	8.33E-08
231478_at	PDE4C	phosphodiesterase 4C, cAMP-specific	3.89515	0.000397385
210096_at	CYP4B1	cytochrome P450, family 4, subfamily B, polypeptide 1	3.76787	9.31E-05
234700_s_at	RNASE7	ribonuclease, RNase A family, 7	3.75572	2.82E-06
219995_s_at	ZNF750	zinc finger protein 750	3.73172	0.000370509
233488_at	RNASE7	ribonuclease, RNase A family, 7	3.69884	2.60E-07
1554333_at	DNAJA4	DnaJ (Hsp40) homolog, subfamily A, member 4	3.67408	0.00706654
Downregulated				
214974_x_at	CXCL5	chemokine (C-X-C motif) ligand 5	−7.51277	0.00489703
227253_at	CP	ceruloplasmin (ferroxidase)	−6.56691	1.09E-07
202018_s_at	LTF	lactotransferrin	−5.95036	0.00041685
226067_at	C20orf114	chromosome 20 open reading frame 114	−5.86084	2.28E-06
204846_at	CP	ceruloplasmin (ferroxidase)	−5.6248	2.85E-07
226147_s_at	PIGR	polymeric immunoglobulin receptor	−5.60813	0.000503421
202376_at	SERPINA3	serpin peptidase inhibitor, clade A (alpha-1 antiproteinase, antitrypsin), membe	−5.5329	3.00E-05
206392_s_at	RARRES1	retinoic acid receptor responder (tazarotene induced) 1	−5.45155	0.000770649
219795_at	SLC6A14	solute carrier family 6 (amino acid transporter), member 14	−5.448	7.24E-05
209813_x_at	TARP	TCR gamma alternate reading frame protein	−5.28045	2.05E-05
1558034_s_at	CP	ceruloplasmin (ferroxidase)	−5.05921	6.79E-10
206391_at	RARRES1	retinoic acid receptor responder (tazarotene induced) 1	−5.02589	0.00013709
216920_s_at	TARP /// TRGC2	TCR gamma alternate reading frame protein /// T cell receptor gamma constant 2	−4.95076	8.60E-05

(*Continued*)

TABLE I. (*Continued*)

Probeset ID	Gene symbol	Gene name	Fold difference	*P*-value
215806_x_at	TARP /// TRGC2	TCR gamma alternate reading frame protein /// T cell receptor gamma constant 2	−4.88084	6.83E-05
205922_at	VNN2	vanin 2	−4.84074	7.05E-06
202357_s_at	CFB	complement factor B	−4.83501	0.00015103
215101_s_at	CXCL5	chemokine (C-X-C motif) ligand 5	−4.80431	0.00109869
205860_x_at	FOLH1	folate hydrolase (prostate-specific membrane antigen) 1	−4.70062	1.60E-05
216623_x_at	TOX3	TOX high mobility group box family member 3	−4.64709	3.19E-05
202833_s_at	SERPINA1	serpin peptidase inhibitor, clade A (alpha-1 antiproteinase, antitrypsin), membe	−4.58774	0.000671618
223721_s_at	DNAJC12	DnaJ (Hsp40) homolog, subfamily C, member 12	−4.51425	9.57E-08
230378_at	SCGB3A1	secretoglobin, family 3A, member 1	−4.48192	1.77E-05
228143_at	CP	ceruloplasmin (ferroxidase)	−4.37586	1.28E-07
215363_x_at	FOLH1	folate hydrolase (prostate-specific membrane antigen) 1	−4.37522	1.15E-05
221872_at	RARRES1	retinoic acid receptor responder (tazarotene induced) 1	−4.3391	0.0022526
204124_at	SLC34A2	solute carrier family 34 (sodium phosphate), member 2	−4.25842	1.65E-06
214774_x_at	TOX3	TOX high mobility group box family member 3	−4.23689	2.67E-05
229659_s_at	–	–	−4.17158	4.41E-06
235229_at	–	–	−4.16726	1.55E-05
209854_s_at	KLK2	kallikrein-related peptidase 2	−4.16369	0.00329434

frequency (≥2). The heat map revealed four distinct patterns that correlated with the four fractionated epithelial subpopulations (TIC, BC, LC, and FC).

In order to better visualize data sets obtained from RNA expression microarray studies, principal component analysis was performed to segregate data based upon functional cellular designations (Fig. 3B). A 3-dimensional scatter plot was derived from the gene list employed for the construction of the hierarchical clustering map. The pattern of samples forming distinct groups is demonstrated using this approach, as previously described [17]. In analyses of 18 samples, putative TIC are easily distinguishable from BC and LC. Although FC demonstrates a distinctive gene expression profile, it is most similar to TIC when evaluated in this context. These results confirm that Epcam/CD44/CD49f cell sorting enables isolation of prostate epithelial subpopulations that are not only functionally distinctive, but exhibit distinct gene expression profiles. The top 30 genes identified as significantly upregulated or downregulated in TIC compared to LC and BC (Table I), with fold difference of expression ranging from 3.67 to 6.99 and *P*-value from 9.87E-09 to 1.65E-04. Probe set identification (ID) for the Affymetrix array is listed in the left column of the table. Uncharacterized genes are listed as "–-" in the gene symbol and gene name columns. Some genes and gene family members identified, such as FILIP1L and RARRES1 had multiple probe sets and are listed more than once.

Validation of Expression Array Data via Quantitative RT-PCR (qRT-PCR)

Validation studies were performed using RT-PCR with TIC, BC, and LC fractions obtained from an independent set of adult prostate specimens (Fig. 4). Representative basal and luminal markers from the gene list, including P63, AR, and PSA were selected, and quantitative RT-PCR was performed with a minimum of three individual patient specimens. Consistent with the Affymetrix gene expression array results, TIC and BC populations demonstrated significant high P63 expression, but relatively low AR and PSA (Fig. 4B). In contrast, LC displayed abundant AR and PSA expression and relatively low levels of P63. These results are consistent with TIC and BC comprising the basal compartment and LC representing epithelial cells from the more differentiated luminal (secretory) compartment.

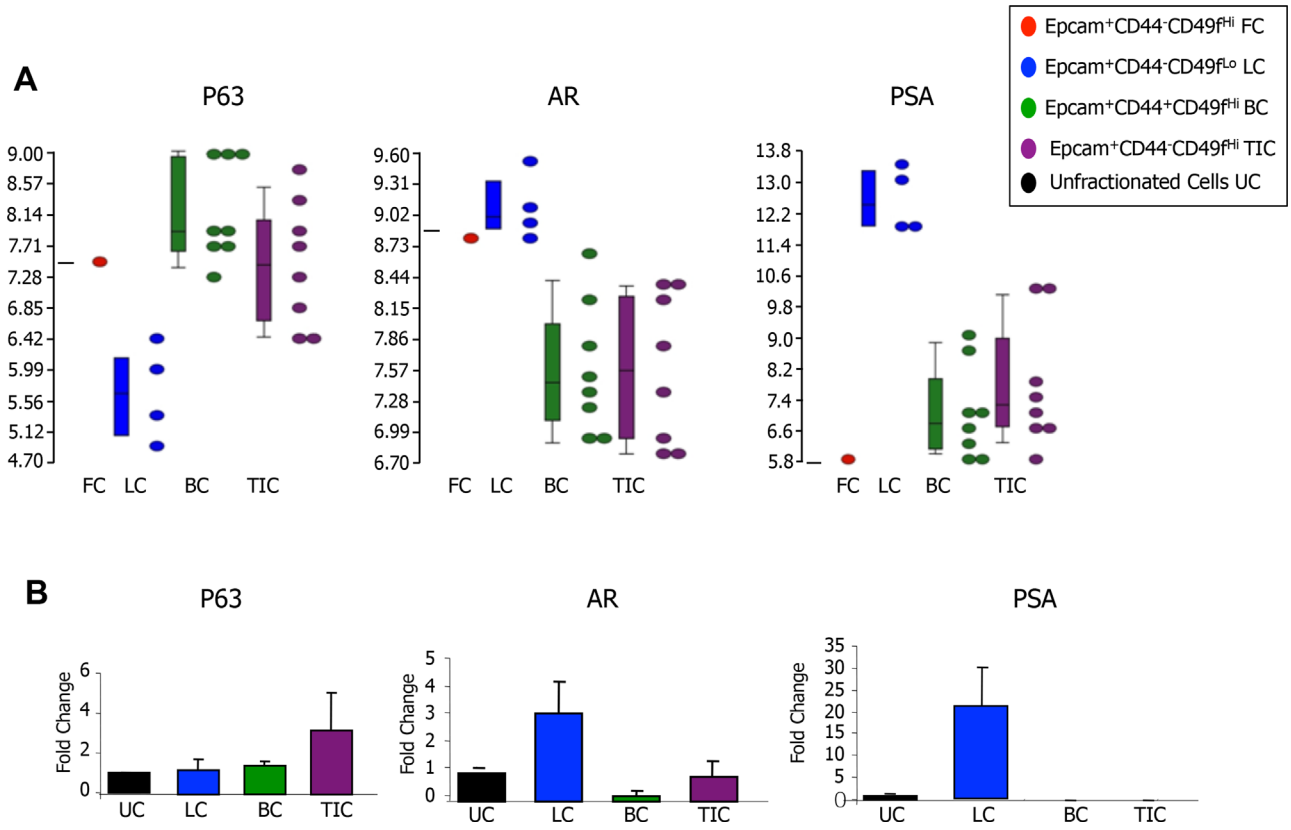

Fig. 4. Validation of select genes differentially expressed among prostate epithelial cell fractions. **A**: Differential expression of the basal marker P63 and luminal markers AR and PSA are demonstrated among the four prostate epithelial populations analyzed (FC—red dot, LC—blue dots, BC—green dots, and TIC—purple dots) in the Affymetrix Gene Chip Human U133 PLUS 2.0 Array analysis. **B**: RNA was isolated from fractionated cells for evaluation via Quantitative RT-PCR. All reactions were performed in triplicate with a minimum of three unique patient specimens. Black columns represent Unfractionated cells (UC), blue columns represent Epcam^{+}CD44^{-}CD49f^{Lo} luminal cells (LC), green columns represent Epcam^{+}CD44^{+}CD49f^{Hi} basal cells (BC), and purple columns represent Epcam^{+}CD44^{-}CD49f^{Hi} tubule-initiating cells (TIC).

Genetic Network and Pathway Analysis of Differentially Expressed Proteins Associated With Adult Prostate Epithelial Populations

To highlight gene expression differences among TIC, BC, and LC that may provide clues about mechanisms underlying specific functional traits associated with each population, analyses were performed with gene lists obtained from comparative analysis of TIC versus BC (total of 1,283 genes) and TIC versus LC (total of 2,316 genes). Characterization of differentially expressed proteins correlating with each gene list was performed using Ingenuity Pathway Analysis (IPA) Version 7.6 software. Genes associated with biological functions in the Ingenuity Pathways Knowledge Base are considered for analysis by defining networks which reveal physical or functional relationships among differentially expressed genes. First, functional groups associated with gene-encoded proteins are identified, followed by determination of statistically enriched pathways that coincide with specific cellular events [16]. IPA analysis demonstrated striking functional group similarities in TIC versus BC (Fig. 5A) and TIC versus LC (Fig. 5B) analyses. Functional groups associated with cancer were of the greatest significance in both datasets. In TIC versus BC analysis, 372 out of 1,283 genes were related to cancer (*P*-value: 1.24E-23–1.38E-03), while 590 out of 2,316 genes were associated with cancer in the TIC versus LC dataset (*P*-value: 7.79E-35–1.95E-03). Other functional groups identified both analyses were associated with reproductive system disease, cell growth and proliferation, cell development, and cell movement.

DISCUSSION

In order for prostate development to occur, interactions between epithelia and mesenchymal cells are necessary to create an organized microenvironment composed of branching ducts/acini that are anchored

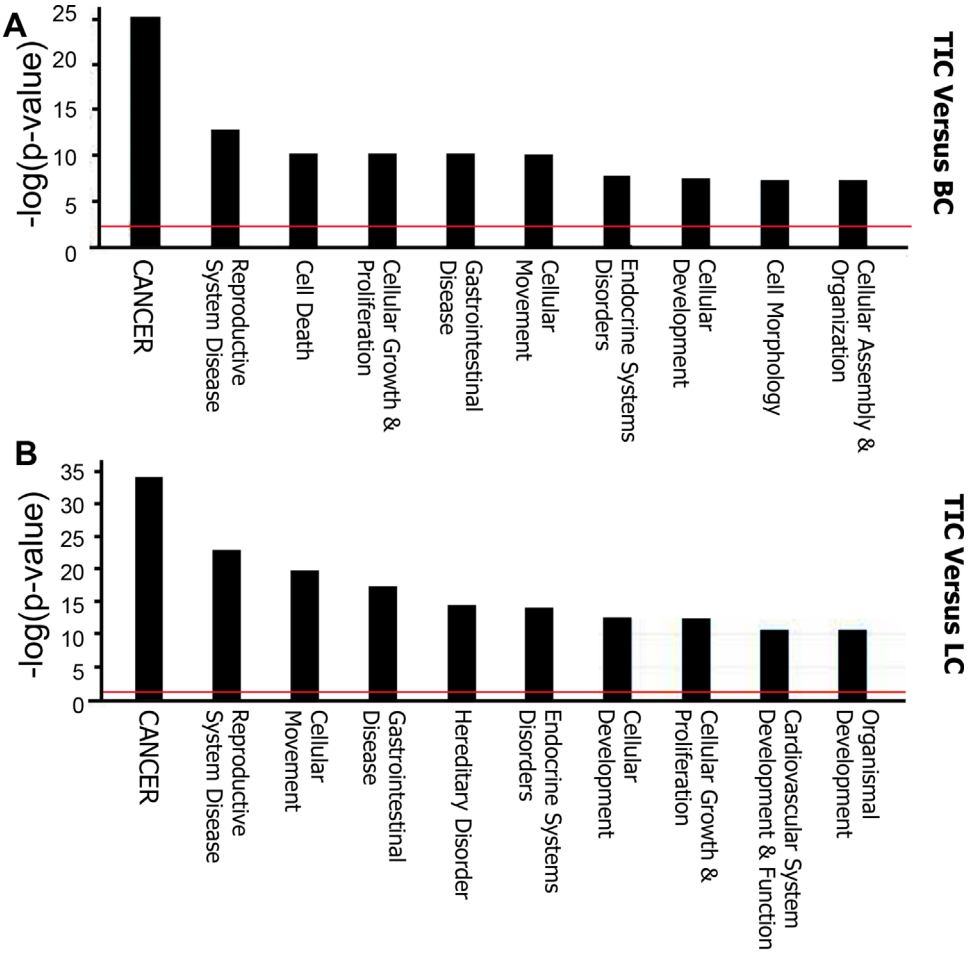

Fig. 5. Gene Ontology analysis of differentially expressed genes between fractionated prostate cells. The top 10 significantly enriched gene ontologies are presented (**A**: TIC vs. BC; **B**: TIC vs. LC).

to a well-vascularized fibromuscular stroma [2]. Similarly, adult prostate tubules populated with basal and luminal epithelial compartments can be induced in vivo, when specific subpopulations that are often referred to as prostate stem cells (PSC) or tubule-initiating cells (TIC) are combined with human fetal prostate stroma (or rodent urogenital sinus mesenchyme) [15]. PSC/TIC survive castrate environments and remain responsive to variations in endocrine/paracrine hormonal cues throughout the lifespan [2,20,21]. In the fetal prostate (12–18 weeks gestation), epithelial buds are precursors to mature canalized ducts/acini [22,23]. In vivo recombination models that utilize adult prostate epithelial appear to replicate natural prostate developmental processes to some degree, since recombinant grafts display rudimentary buds interspersed among differentiated, multi-layered, secretion-filled tubules [15].

The epithelial-stromal interactions that define fetal development and persist into adulthood are likely perturbed in prostate tumorigenesis, leading to disorganized branching morphogenesis [2]. Prostate adenocarcinomas are typically identified and graded based upon the degree of breakdown of glandular architecture. Ranging from tightly clustered luminal cell outgrowths with small lumens to sheets of amorphous cells, all tumor foci appear to lose the basal cell layer [24]. Deciphering the mechanisms used by TIC to regulate branching morphogenesis and cellular differentiation throughout fetal and adult prostate development may yield important clues to uncover durable treatments for invasive carcinoma.

Previous prostate tissue regeneration studies performed with fractionated adult murine and human epithelial cells identified subpopulations adept at inducing tubule formation [5,9,15,25]. Epithelial cells with the most efficient tubule-initiating capability consistently appear to originate from the basal compartment. Although loss of basal cells is a hallmark of adenocarcinoma, cells from the basal compartment are capable of malignant transformation and induce luminal cancer foci when transduced with oncogenes [7,11].

It is conceivable that prostate cancers co-opt traits of basal TIC that could impart invasion and survival advantages. In this report, we have characterized benign human prostate cells from fetal and adult specimens via antigenic profiling (IHC and FACS) and microarray analysis. In addition, we have demonstrated the tubule-initiating capability of $Epcam^{+}CD44^{-}$ fetal prostate cells, which appear to be the developmental counterpart to $Epcam^{+}CD44^{-}$/$Epcam^{+}CD44^{-}CD49f^{Hi}$ adult primary prostate cells with similar functional capabilities, although the frequency of the grafts with tubules retrieved from fetal epithelial fractions was relatively low (25%). Microarray analysis has illuminated molecular and genetic pathways common to TIC at the fetal and adult stages of development and identified processes associated with tumorigenesis that may be targeted in future studies.

IHC and FACS analysis demonstrated differences in basal/luminal marker expression among cells composing prostatic ducts/acini in fetal versus adult prostate tissue. Similarities were found with regard to the antigenic profile of epithelial populations capable of efficient tubule-initiation in vivo isolated from fetal and adult prostate specimens. TIC possesses an $Epcam^{+}CD44^{-}$ antigenic profile and co-express basal markers CK5 and P63. The nuance of CD44 negativity of adult TIC is interesting, since IHC analysis reveals that the majority of adult prostate basal epithelia appear to express CD44 (see Fig. 1A). In human fetal prostate tissue, the vast majority of cells detected via IHC were $CD44^{-}$ and only a minute population of $CD44^{+}$ cells (0.01%) could be detected via FACS analysis of total cells recovered from pooled dissociated fetal prostate tissues. Despite pooling to increase cellular yield, it was only possible to obtain on the order of 10^3 epithelial cells via cell sorting. Consequently, isolating the $Epcam^{+}CD44^{+}$ subpopulation for functional evaluation in tissue recombination assays was a challenge and a limitation for our current study. Additionally, we were unable to stratify cells based on $CD49f^{Hi}$ expression, similar to the adult TIC population. However, since $Epcam^{+}CD44^{-}$ fetal prostate clearly demonstrated TIC activity, in contrast to the $Epcam^{-}CD44^{-}$ population, it can be concluded that this fraction is functionally similar to its adult counterpart in its tubule-initiating activity. We show here that a nearly pure population of $Epcam^{+}CD44^{-}$ cells comprises the fetal epithelial compartment at a stage of development when these cells are poised to commence unprecedented growth and differentiation in response to rising testosterone levels. This epithelial profile is compatible with tubule-initiating and branching morphogenesis capabilities previously demonstrated in studies with fractionated adult prostate tissue. The notable shift in $Epcam^{+}CD44^{-}$ cells from fetal majority to representing a small minority in adult prostate tissues, is in line with previous studies suggesting that stem cells are rare in adult tissues, with a small pool in reserve to perform tissue repair/regeneration as needed.

Interesting similarities between fetal and adult TIC were also evident from the microarray analysis performed. The expression profile of FC appeared closest to adult TIC, compared to BC and LC, and the genes most differentially expressed in adult TIC are associated with cancer. One limitation to the microarray analysis is the limited amount of RNA obtained from the fetal tissues. In order to perform this analysis six dissociated fetal samples were pooled prior to cell sorting. As a result of the limited cell retrieval, individual fetal samples or multiple pooled fetal samples were not available for comparative analysis. Despite this limitation, the pooled fetal sample displayed an expression profile most similar to adult TIC, consistent with the IHC profile and functional overlap of these developmentally distinct populations. IPA analysis of TIC included pathways involved in androgen and estrogen metabolism, ERK/MAPK signaling, Wnt/B-catenin signaling, and human embryonic stem cell pluripotency. This first--in-field gene expression analysis of fractionated prostate epithelial cells associated with specific biological functions will be useful in determining molecular pathways involved in the transformation process and castration-resistant survival and growth.

CONCLUSION

Our results indicate that both fetal and adult prostate tubule-initiating cells display clustering gene expression profiles. The genes and pathways common to these cell populations are often deregulated in cancer, which may suggest a cell-of-origin role for TIC in tumor initiation.

ACKNOWLEDGMENTS

Flow cytometry/FACS was performed in the UCLA Jonsson Comprehensive Cancer Center (JCCC) and is supported by National Institutes of Health awards CA-16042 and AI-28697, and by the JCCC, the UCLA AIDS Institute, and the David Geffen School of Medicine at UCLA. Procurement of fetal tissues is supported by the Center for AIDS Research at UCLA. We gratefully thank the genitourinary pathologists and technicians in the UCLA Tissue Procurement Clinical Laboratory as well as those at the Greater Los Angeles Veterans Hospital for assisting with specimen retrieval and slide review. Support for this study was provided by the Prostate Cancer Foundation (Young

Investigator and Challenge awards), the Jean Perkins Foundation, the Department of Defense (PC07373), NIH U54 CA 143931, and the Margaret E. Early Medical Research Trust. Thanks to Lihong Huo for manuscript review.

REFERENCES

1. Barnett DH, Huang HY, Wu XR, Laciak R, Shapiro E, Bushman W. The human prostate expresses sonic hedgehog during fetal development. J Urol 2002;168:2206–2210.
2. Cunha GR, Ricke W, Thomson A, Marker PC, Risbridger G, Hayward SW, Wang YZ, Donjacour AA, Kurita T. Hormonal, cellular, and molecular regulation of normal and neoplastic prostatic development. J Steroid Biochem Mol Biol 2004;92: 221–236.
3. Timms BG. Prostate development: A historical perspective. Differentiation 2008;76:565–577.
4. Letellier G, Perez MJ, Yacoub M, Levillain P, Cussenot O, Fromont G. Epithelial phenotypes in the developing human prostate. J Histochem Cytochem 2007;55:885–890.
5. Garraway IP, Sun W, Tran CP, Perner S, Zhang B, Goldstein AS, Hahm SA, Haider M, Head CS, Reiter RE, Rubin MA, Witte ON. Human prostate sphere-forming cells represent a subset of basal epithelial cells capable of glandular regeneration in vivo. Prostate 2010;70:491–501.
6. Isaacs JT, Coffey DS. Etiology and disease process of benign prostatic hyperplasia. Prostate Suppl 1989;2:33–50.
7. Xin L, Lawson DA, Witte ON. The Sca-1 cell surface marker enriches for a prostate-regenerating cell subpopulation that can initiate prostate tumorigenesis. Proc Natl Acad Sci USA 2005;102:6942–6947.
8. Xin L, Lukacs RU, Lawson DA, Cheng D, Witte ON. Self-renewal and multilineage differentiation in vitro from murine prostate stem cells. Stem Cells 2007;25:2760–2769.
9. Burger PE, Xiong X, Coetzee S, Salm SN, Moscatelli D, Goto K, Wilson EL. Sca-1 expression identifies stem cells in the proximal region of prostatic ducts with high capacity to reconstitute prostatic tissue. Proc Natl Acad Sci USA 2005;102:7180–7185.
10. Dontu G, Liu S, Wicha MS. Stem cells in mammary development and carcinogenesis: implications for prevention and treatment. Stem Cell Rev 2005;1:207–213.
11. Goldstein AS, Huang J, Guo C, Garraway IP, Witte ON. Identification of a cell of origin for human prostate cancer. Science 2010;329:568–571.
12. Singh S, Dirks PB. Brain tumor stem cells: Identification and concepts. Neurosurg Clin N Am 2007;18.
13. Kim CF, Jackson EL, Woolfenden AE, Lawrence S, Babar I, Vogel S, Crowley D, Bronson RT, Jacks T. Identification of bronchioalveolar stem cells in normal lung and lung cancer. Cell 2005;121:823–835.
14. Choi N, Zhang B, Zhang L, Ittmann M, Xin L. Adult murine prostate basal and luminal cells are self-sustained lineages that can both serve as targets for prostate cancer initiation. Cancer Cell 2012;21:253–265.
15. Guo C, Liu H, Zhang BH, Cadaneanu RM, Mayle AM, Garraway IP. Epcam, CD44, and CD49f distinguish sphere-forming human prostate basal cells from a subpopulation with predominant tubule initiation capability. PLoS ONE 2012; e34219.
16. Li X, Wang H, Touma E, Rousseau E, Quigg RJ, Ryaby JT. Genetic network and pathway analysis of differentially expressed proteins during critical cellular events in fracture repair. J Cell Biochem 2007;100:527–543.
17. Koh SS, Wei JP, Li X, Huang RR, Doan NB, Scolyer RA, Cochran AJ, Binder SW. Differential gene expression profiling of primary cutaneous melanoma and sentinel lymph node metastases. Mod Pathol 2012;25:828–837.
18. Robinson EJ, Neal DE, Collins AT. Basal cells are progenitors of luminal cells in primary cultures of differentiating human prostatic epithelium. Prostate 1998;37:149–160.
19. Tran CP, Lin C, Yamashiro J, Reiter RE. Prostate stem cell antigen is a marker of late intermediate prostate epithelial cells. Mol Cancer Res 2002;1:113–121.
20. Hayward SW, Haughney PC, Rosen MA, Greulich KM, Weier HU, Dahiya R, Cunha GR. Interactions between adult human prostatic epithelium and rat urogenital sinus mesenchyme in a tissue recombination model. Differentiation 1998;63:131–140.
21. Risbridger GP, Taylor RA. Minireview: Regulation of prostatic stem cells by stromal niche in health and disease. Endocrinology 2008;149:4303–4306.
22. Xue Y, Smedts F, Ruijter ET, Debruyne FM, de la Rosette JJ, Schalken JA. Branching activity in the human prostate: A closer look at the structure of small glandular buds. Eur Urol 2001;39:222–231.
23. Lunacek A, Oswald J, Schwentner C, Schlenck B, Horninger W, Fritsch H, Longato S, Sergi C, Bartsch G, Radmayr C. Growth curves of the fetal prostate based on three-dimensional reconstructions: A correlation with gestational age and maternal testosterone levels. BJU Int 2007;99: 151–156.
24. Epstein JI. An update of the Gleason grading system. J Urol 2010;183:433–440.
25. Goldstein AS, Lawson DA, Cheng D, Sun W, Garraway IP, Witte ON. Trop2 identifies a subpopulation of murine and human prostate basal cells with stem cell characteristics. Proc Natl Acad Sci USA 2008;105:20882–20887.